Excitation Functions, Recoil Ranges, and Statistical Theory Analysis of Reactions Induced in Fe^{56} with 6–29-MeV He^3 Ions*

JEAN-PIERRE HAZAN† AND MARSHALL BLANN
Department of Chemistry, The University of Rochester, Rochester, New York
(Received 2 October 1964; revised manuscript received 16 November 1964)

Excitation functions and integral recoil ranges have been measured for products of the (He^3,p), (He^3,pn), (He^3,$p2n$), (He^3,$2n$), and (He^3,$3n$) reactions of Fe^{56}. The He^3 kinetic energies varied between 6 and 29 MeV. Targets were 99.7% enriched Fe^{56}, electroplated on 0.2-mil gold foils. The experimental recoil ranges of reaction products formed between the corresponding reaction thresholds and excitation function peaks are compared with the ranges predicted by the theory of Lindhard, Scharff, and Schiøtt; the ranges are in agreement with the theoretical predictions within the ±10% uncertainty of the experimental measurements. With the exception of the Co^{57} ranges resulting from He^3 ion bombardment at energies greater than 25 MeV, all ranges are consistent with a predominantly full-momentum-transfer mechanism with 90° symmetry for emitted particles. The sensitivity of the experimental ranges to reaction mechanism is discussed, as is the influence on range of nucleon evaporation. The excitation functions for the production of Ni^{56}, Co^{56}, Ni^{57}, Co^{57}, and Co^{58} have been compared with three sets of statistical-theory calculations. The first set of calculations was a conventional Weisskopf evaporation calculation in which a level density of the form $\rho(E,J) \propto (2J+1)\,E^{-2}\exp[2(aE)^{1/2}]$ was used. The calculated excitation functions attained their maximum yields at lower energies than the corresponding experimental excitation functions, as had been noted for similar calculations for He^4-induced reactions of Fe^{56} and Ni^{58}. A correlation is shown to exist between the displacement of calculated and experimental excitation functions and average rotational energy for the three systems. In the second set of calculations a level density of the form $\rho(E,J) \propto (2J+1)\,(E-E_{\mathrm{ROT}})^{-2}\exp\{2[a(E-E_{\mathrm{ROT}})]^{1/2}\}$ was used, where $E_{\mathrm{ROT}}=J(J+1)\hbar^2/2\,I_{\mathrm{RIG}}$, and I_{RIG} is the rigid-body moment of inertia. Evaporation probabilities were summed for each impact parameter J, weighted as $(2J+1)T_J$, where T_J is the transmission coefficient for a He^3 ion introducing J units of orbital angular momentum. Transmission coefficients were calculated with the nuclear optical model. It was assumed that all rotational energy was dissipated by γ-ray deexcitation. The second set of calculated excitation functions was in better agreement with experimental values with respect to the positions of maxima on the energy axis. In the third set of calculations a level density of the form $\rho(E,J) \propto (2J+1)\,(E+\Delta E)^{-2}\exp\{2[a(E+\Delta E)]^{1/2}\}$ was used, where ΔE was a shift in energy calculated according to the model of Rosenzweig in order to approximate the influence of shell occupation on level densities. Ratios of yields of Co^{56}/Ni^{56} and Co^{57}/Ni^{57} calculated in the third set of calculations were in approximately an order of magnitude better agreement with experimental values than the results of the first set of calculations. Energies used in all calculations were corrected for pairing effects using the masses of Everling *et al.*; optical-model nonelastic cross sections were used for inverse-reaction cross sections, and the level spacing parameter a was evaluated from Fe^{56}(He^3,p) proton spectra.

I. INTRODUCTION

THE He^3 projectile is potentially valuable for studying the influence of angular momentum on the decay of highly excited nuclei. This follows from the very high Q value for He^3 induced reactions (15.5 MeV for the reactions to be described in this work)[1] compared with He^4-induced reactions on the same targets (6.3 MeV). Whether such a loosely bound particle as He^3 will react predominantly by a compound nucleus mechanism, or whether it will react mainly by pickup and stripping mechanisms, is yet an open question. This work is part of an investigation intended to answer the latter question for He^3-induced reactions in the iron region, and for He^3 kinetic energies of 6–29 MeV (excitation energies of 21–44 MeV).

Where only a single particle may be emitted, angular distributions and spectral measurements give the most detailed information on reaction mechanisms; consequently, proton spectra and angular distributions were measured for the Fe^{56}(He^3,p) reaction induced with 10-MeV He^3 ions.[2] Analysis of these data in the region of one-particle emission indicated reactions proceeding predominantly by a compound-nucleus mechanism. The Fe^{56}(He^3,$xpyn$) reactions were next measured at incident He^3 energies of 6–29 MeV. Where multiple-particle emission takes place angular distribution information applies only to the average process; it does not give information on any specific reaction path. To obtain information on reaction mechanisms for production of specific products, we have measured the mean recoil ranges of those products, and the corresponding excitation functions. In this paper, we report the results of the recoil range and excitation function measurements, followed by an application of the statistical theory[3–5] of nuclear reactions to those excitation functions having recoil ranges consistent with a compound nucleus mechanism, in order to test the hypothesis of statistical equilibrium for those reactions. In particular, we are interested in the influence of angular momentum and nuclear shell structure in the decay of compound nuclei.

* This work was supported by the U. S. Atomic Energy Commission.
† Present address: 146 rue de Tocquiville, Paris, France.
[1] F. Everling, L. A. Koenig, J. H. E. Mattauch, and A. H. Wapstra, *1960 Nuclear Data Tables, Part 1* (U. S. Government Printing Office, Washington, D. C., 1960).
[2] J. Hazan, thesis, University of Rochester, 1964 (unpublished).
[3] V. F. Weisskopf, Phys. Rev. **52**, 295 (1937).
[4] H. A. Bethe, Rev. Mod. Phys. **9**, 69 (1937).
[5] V. F. Weisskopf and D. H. Ewing, Phys. Rev. **57**, 472 (1940).

II. EXPERIMENTAL PROCEDURES

A. Targets

The Fe^{56} targets (99.7% enrichment) were electroplated onto 0.2-mil gold foils using the basic tartrate method previously described.[6] The plating was done in a 1.9-cm-diam glass chimney. Target thicknesses varied between 2 and 3 mg/cm^2. The gold backings varied in general by less than 3% from the average of 12.1 mg/cm^2; nonetheless, each foil was individually measured and weighed prior to use. In the first bombardment the last two backing foils were 7.0 mg/cm^2 gold foil.

Foil stacks were prepared with 0.25-mil (1.98 to 2.02 mg/cm^2) aluminum catcher foils downstream from each Fe^{56} target. The first target stack contained 13 such target-catcher pairs, the second stack contained 12. Each target stack was wrapped in a single layer of 0.25-mil Al foil for ease in handling.

B. Bombardments

Two bombardments were made at the Yale University Heavy Ion Accelerator. The beam energy, as determined by magnetic analysis, was 30.5±0.4 MeV in both irradiations. The beam passed through analyzing and bending magnets before striking the target stack. A $\frac{1}{4}$-in. collimator was placed 10 in. in front of the targets (target diameter was $\frac{3}{4}$ in.). Target holders served as Faraday cups; current integrator readings indicated beams of 0.36 μA-h and 0.56 μA-h for the two bombardments.

C. Chemical Separations

Target and catcher foils were dissolved separately with the necessary carriers, including Mn holdback carrier. The chemical procedures by which Ni, Co, Fe, and Mn fractions were separated have been discussed previously.[7]

All cobalt yields were determined colorimetrically by the thiocyanate method (after all radiation detection was completed).[8] Nickel yields were determined gravimetrically as the dimethylglyoxime salt.

D. Radiation Detection

The characteristics of radiation detected in cross section and recoil-range determinations of this work are summarized in Table I. Where positrons were detected, calibrated end-window porportional counters were used.[9,10] For γ-ray scintillation spectrometry, 1-$\frac{1}{2}$×1 in. and 3×3 in. NaI(Tl) crystals were used with a 256-channel pulse-height analyzer. Efficiency curves due to Wolicki *et al.* and Heath were used to obtain crystal efficiencies.[11,12] Coincidence corrections were applied where appropriate.

TABLE I. Decay characteristics of isotopes studied in this work.[a]

Nuclides	Type of radiation observed	Energy of radiation observed (MeV)	Assumed abundance (per decay)	Assumed half-life
Ni^{56}	γ	0.164	0.99	6.1 days[b]
Ni^{57}	β^+		0.50	36.0 h
Co^{56}	γ	1.26	0.70	77 days
Co^{57}	γ	0.120	1.00	270 days
Co^{58}	γ	0.810	1.00	71 days[c]

[a] D. Strominger, J. M. Hollander, and G. T. Seaborg, Rev. Mod. Phys. **30**, 585 (1958) unless otherwise referenced.
[b] D. O. Wells, S. L. Blatt, and W. E. Meyerhof, Phys. Rev. **130**, 1961 (1963).
[c] The 0.810-MeV photopeak area represented the yield of Co^{56} and Co^{58}. The fraction of the peak due to Co^{16} was calculated from the area of the 1.26-MeV peak and subtracted from the total 0.810-MeV peak area to obtain the Co^{58} contribution.

E. Errors

In general, errors in cross-section determinations are greater than errors in recoil-range determination, since in the former case the result is dependent upon absolute counting and beam-current measurement, while in the latter case only relative intensities of a given type of radiation are involved. In the following paragraphs we discuss the estimated errors in cross sections and recoil ranges for each isotope measured.

The precision estimates given for photopeak integration result from the reproducibility of integration of multiplicate spectra, and therefore reflect both the counting statistics and uncertainties due to Compton scattering background from higher energy γ rays. The errors given for the recoil ranges determined by γ-ray spectrometry include both an uncertainty for the precision of photopeak integration, and for the chemical yields in target and catcher foils. Errors estimated for the corresponding cross sections also include estimates of errors due to beam-current measurement (±10%) and conversion of activities to disintegration rate. Where β^+ counting was used (Ni^{57}) the error estimates for recoil ranges are based on variations in efficiency due to sample thickness and on chemical yields; for cross sections an uncertainty for absolute counting and beam-current measurement has also been included. The estimates of error cited are intended to be approximately 90% confidence limits. A more detailed discussion of the absolute calibration of counting equipment used and the reproducibility involved may be found elsewhere.[10]

Ni^{56}. Nickel-56 activities were determined by observing the 0.164-MeV γ-ray photopeak. Spectra were measured 8–9 days after each bombardment, at which time Ni^{57} activity had decreased to ≈2% of the original

[6] M. Blann, F. M. Lanzafame, and R. A. Piscitelli, Phys. Rev. **133**, B700 (1964).
[7] M. Blann and A. Ewart, Phys. Rev. **134**, B783 (1964).
[8] F. D. Snell and C. T. Snell, *Colorimetric Methods of Analysis* (D. Van Nostrand Company, New York, 1949), 3rd ed., p. 361.
[9] B. P. Bayhurst and R. J. Prestwood, Nucleonics **17**, 82 (1959).
[10] M. Blann, University of California Lawrence Radiation Laboratory Report No. UCRL-9190 (unpublished).
[11] E. A. Wolicki, R. Jastrow, and F. Brooks, Navy Research Laboratory Report NRL-4833, 1956 (unpublished).
[12] R. L. Heath, Atomic Energy Commission Research and Development Report IDO-16408, 1957 (unpublished).

value. The 0.120-MeV photopeak due to Co^{57} was, in general, well resolved from the 0.164-MeV photopeak. Samples having too low an activity to give a well-resolved peak were not included in the final results. An escape peak correction was applied using values due to Axel.[13] Precision in measuring the 0.164-MeV photopeak was 5–7% for target samples and 7–10% for samples from catcher foils. The recoil ranges should therefore be accurate to ±15%; cross sections should be accurate to ±25%.

Ni^{57}. Nickel-57 yields were determined by β^+ counting; decay was followed for 4 to 5 half-lives with no significant deviation from a 36-h half-life. Corrections to counting rates due to variations in sample thickness were applied, and found to be less than 5%. We estimate the recoil ranges calculated for Ni^{57} are accurate to ±8%; cross sections should be accurate to ±20%.

Co^{56}. Cobalt-56 was determined from the activity of the 1.26-MeV γ-ray photopeak using a 3×3-in. NaI crystal as detector. Standard spectral peaks were used to subtract contributions due to high-energy photopeaks and their associated Compton distributions. The precision of this photopeak integration process was of the order of ±10%. Recoil ranges should be accurate to ±15%, cross sections to ±25%.

Co^{57}. The 0.120-MeV γ-ray photopeak of Co^{57} was observed using a 1-½×1-in. NaI crystal. The precision of photopeak integration was of the order of 3–5%. We estimate the recoil range accuracy to be of the order of ±8%; cross sections should be accurate to ±20%.

Co^{58}. Cobalt-58 yields were determined from the area of the 0.810-MeV γ-ray peak. Since Co^{56} decay also contributes to the 0.810-MeV photopeak, a correction was applied based on the area of the 1.26-MeV Co^{56} photopeak, and the intensity factors given in Table I. Consequently, at higher energies where Co^{58} cross sections were getting small with respect to Co^{56} cross sections, the yields of Co^{58} had to be obtained as the difference between two nearly equal numbers. For this reason we have not calculated Co^{58} cross sections for incident He^3 energies above 21 MeV, nor have we calculated Co^{58} recoil ranges for incident He^3 energies above 19 MeV. We estimate recoil range accuracy to be ±10% for incident He^3 energies less than 15 MeV, and ±20% at 19 MeV. Cross sections should be accurate to ±25–30%.

F. He^3 Range-Energy Determination

The He^3 kinetic energy as a function of target depth was determined by using the range-energy calculations of Williamson and Boujot for He^3 in Fe, Au, and Al.[14] The energies quoted are those calculated at the center of the targets. Deviations from the mean energy due to target thickness were typically ±0.30 MeV at 9 MeV, ±0.25 MeV at 11 MeV, ±0.20 MeV at 16 MeV, and ±0.15 MeV at 29 MeV.

Errors due to energy determination as a function of target depth are due to the uncertainty in range-energy relationships and errors in foil thickness determination. The error increases progressively as one proceeds down the stack. The energy down to 11 MeV is estimated to be accurate to within ±1 MeV; below 11 MeV the degradation of the beam increases rapidly, and the uncertainty may attain 1.5–2.0 MeV at 6 MeV.

G. Recoil Range Determination

The thick-target–thick-catcher method was used in this work to measure mean recoil ranges projected in the beam direction. This is accomplished by measuring the fraction f of the activity of a given isotope in the catcher foil,

$$f=A_c/(A_c+A_t),$$

where A_t is the activity of the isotope in the target foil and A_c is the activity in the catcher foil.

The relationship of the fraction of the activity in the catcher foil to the recoil range is as follows:

Assume a target of thickness 0 at the downstream (with respect to the beam) surface, and T at the upstream surface. Let t represent the thickness coordinate, i.e., $0\leq t\leq T$. Assume that the cross section for formation of the isotope of interest at depth, t in the target is

$$\sigma_t=\frac{(\sigma_T-\sigma_0)t}{T}+\sigma_0, \tag{1}$$

where σ_T and σ_0 represent the cross sections at the upstream and downstream surfaces of the target, respectively. If it is assumed that all ions formed within their range, R, of the downstream surface of the target will escape from the target (and therefore be found in the catcher foil), then

$$f=\frac{A_c}{A_c+A_t}=\frac{\int_0^R \sigma_t dt}{\int_0^T \sigma_t dt}=\frac{R}{T^2}\frac{2\sigma_0 T+(\sigma_T-\sigma_0)R}{(\sigma_0+\sigma_T)}, \tag{2}$$

where σ_t is given by Eq. (1). We have used two simplified forms of Eq. (2) in calculating the recoil ranges of this work. The first was for situations where $\sigma_T=\sigma_0$, yielding

$$R=fT. \tag{3}$$

The second form used was for situations where σ_0 was not equal to σ_T, but where the difference between σ_0 and σ_T was less than σ_0. Under these conditions (since $R\ll T$)

$$R=fT\frac{\sigma_{av}}{\sigma_0}, \tag{4}$$

where $\sigma_{av}=(\sigma_0+\sigma_T)/2$. The linear approximation of Eq.

[13] P. Axel, Rev. Sci. Instr. **25**, 391 (1954).
[14] C. Williamson and J. P. Boujot, Centre D'Etudes Nucléaires de Saclay, France, CEA No. 2189, 1962 (unpublished).

TABLE II. Cross sections and recoil ranges measured in this work.

He^3 Kinetic energy[a]	t[b]	Co^{56} σ[c]	Co^{56} $\bar{R}$[d]	Ni^{56} σ[c]	Ni^{56} $\bar{R}$[d]	Co^{57} σ[c]	Co^{57} $\bar{R}$[d]	Ni^{57} σ[c]	Ni^{57} $\bar{R}$[d]	Co^{58} σ[c]	Co^{58} $\bar{R}$[d]
29.3	2.60	280	0.32	2.1	0.33	280	0.24	12	0.28		
29.3[e]	2.50	210	0.35	1.7	0.34	230	0.24	11	0.30		
27.8	3.00	310	0.22	2.3	0.25	370	0.17	18	0.22		
27.8[e]	2.86	220	0.29	1.7	0.29	280	0.22	15	0.27		
26.3	3.07	210	0.32	1.4	0.32	320	0.26	17	0.29		
26.3[e]	2.40	190	0.29	1.3	0.28	330	0.23	16	0.28		
24.7	2.49	200	0.25	1.3	0.29	450	0.24	24	0.26		
24.1[e]	2.57	130	0.29	0.98	0.30	340	0.28	24	0.28		
23.1	1.97	140	0.26	0.92	0.29	470	0.26	28	0.29		
22.3[e]	1.37	91	0.26	0.79	0.27	470	0.23	31	0.26		
21.5	1.90	74	0.27	0.67	0.28	500	0.26	33	0.31	19	
20.6[e]	3.31	59	0.19	0.50		650	0.19	50	0.21	25	
19.8	2.06	40	0.22	0.35		630	9.23	44	0.26	25	
18.7[e]	1.73	17	0.25			560	0.23	44	0.24	24	0.16_0
18.0	1.48	14	0.22			680	0.22	48	0.24	26	0.17_0
16.7[e]	2.49					680	0.18	49	0.19	30	0.15_3
16.0	2.78					600	0.21	39	0.23	27	0.18_0
14.4[e]	2.54					610	0.16_7	39	0.17_7	38	0.15_5
13.7	2.24					440	0.17_0	26	0.17_5	29	0.17_3
11.8[e]	2.38					440	0.14_8	27	0.14_3	44	0.15_0
11.2	2.67					430	0.14_0	25	0.15_4	46	0.17_0
9.2	2.90					230	0.13_0	14	0.12_0	47	0.13_0
9.1[e]	2.61					170	0.13_4	11	0.11_5	38	0.12_4
6.5	2.88					43	0.08	2.4	0.06	7	0.08_5
5.7[e]	2.25					8.0				4	

[a] He^3 kinetic energy (MeV) at center of target.
[b] Target "thickness" (mg/cm²).
[c] Cross section (mb).
[d] Average range projected in the beam direction (mg/cm²).
[e] Second bombardment.

(1) was valid for all points measured in this work, so that Eqs. (3) and (4) were valid as used.

The recoil ranges and cross sections measured in this work are summarized in Table II.

III. DEPENDENCE OF RECOIL RANGES ON REACTION MECHANISMS

In the following sections we will compare excitation functions of this work with the predictions of the statistical theory. Such a comparison would be meaningless if the preponderate contributions to a given cross section resulted from partial momentum transfer reactions, or reactions in which the emitted particles were strongly peaked in the forward direction. We therefore use the recoil ranges of specific product nuclides to show which reactions are consistent with a mechanism of full-momentum transfer followed by particle emission which is symmetric about 90° c.m. To do so requires a theoretical range-energy relation for heavy ions, consideration of the accuracy of the range-energy relation, of the influence of nucleon evaporation on the range expectation, and of the sensitivity of the range to asymmetric particle emission. These details will be discussed in this section.

A. Theoretical Ranges

The theoretical range relationship used was due to Lindhard, Scharff, and Schiøtt (hereafter referred to as LSS).[15] Their results are presented as a universal set of range-energy curves, from which we have calculated ranges for recoil ions of $Z=27$, $A=56$ in $_{26}Fe^{56}$; the difference in ranges calculated for any product of this work and the average product (Co^{56}) does not exceed 3%. Corrections for scattering (calculated by LSS) were applied to get ranges projected in the beam direction. We wish to compare the theoretical range curve with experimental ranges of recoil products having known momenta.

At reaction thresholds, reaction products must have received the full momentum of the incident ion, i.e.,

$$E_R = E_B[M_B/(M_T+M_B)][M_R/(M_T+M_B)],$$

where E_R is the recoil ion kinetic energy, E_B is the incident ion kinetic energy, M_B is the mass of the incident ion, M_T is the target ion mass, and M_R is the mass of the recoil ion. We have, therefore, chosen to compare ranges from the region of reaction thresholds to excitation function peaks with the theoretical predictions. We expect these products to represent full (or very nearly full) momentum transfer due to considerations of available energy. Results of the comparison are shown in Fig. 1 both for He^3 and He^4-induced reactions of Fe^{56}.[16] The experimental ranges shown in Fig. 1 have been corrected (3–18%) for the influence of nucleon evapora-

[15] J. Lindhard, M. Scharff, and H. E. Schiøtt, Kgl. Danske Videnskab. Selskab, Mat. Fys. Medd. **33**, No. 14 (1963).
[16] A. Ewart and M. Blann, Bull. Am. Phys. Soc. **9**, 471 (1964).

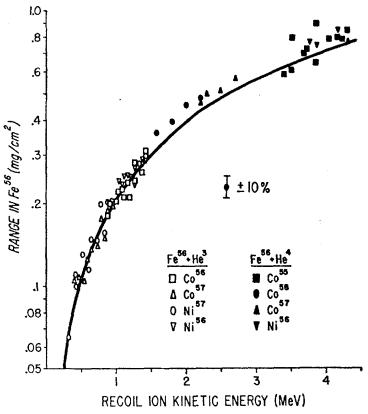

FIG. 1. Comparison of experimental recoil ranges with the values predicted by the range-energy theory of Lindhard *et al.* The points shown represent ranges of products formed between the corresponding reaction thresholds and excitation-function peaks. The experimental ranges have been corrected for the influence of nucleon emission as discussed in Sec. III. The error flag represents the ±10% average uncertainty estimated for the experimental ranges.

tion on range, as will be discussed shortly. If the products shown in Fig. 1 did not result from reactions proceeding by a mechanism involving full momentum transfer, points representing given isotopes would be expected to curve away from the locus of ranges of products nearest to reaction thresholds. Since this is not the case, we conclude that within our experimental uncertainties, the experimental ranges of Fig. 1 do represent full-momentum transfer reactions, and the theoretical range-energy relationship is correct to ±10% over the region of interest.

B. Influence of Nucleon Emission on Recoil Ranges

For the recoil energies of interest in this work, the range is not proportional to momentum. Consequently, the average range will be changed by nucleon evaporation. We wish to compare the experimental ranges with the theoretical expectation for a reaction proceeding by the compound nucleus mechanism; we therefore wish to recalculate range-energy curves for each reaction studied, where we assume an isotropic evaporation spectrum for all nucleons emitted. Such a calculation would, unfortunately, be extremely tedious in situations where more than a single nucleon was emitted. In a somewhat analogous situation, where α particles were emitted from a recoiling compound nucleus, it was shown that replacement of an evaporation spectrum with an average energy made very little difference (actually $<1\%$) in the value of the average range.[7] This is also true for nucleon emission in this work. It was also shown in the case of α emission that the range changed very little ($<7\%$) if the α-particle angular distribution was peaked 50% forward and 50% backward rather than being isotropic.[7] Again, the same arguments are valid for nucleon emission in this work. We have, therefore, used average evaporation energies (from a statistical theory calculation) of 3 MeV for neutrons and 6 MeV for protons and assumed an angular distribution in which 50% of the particles were emitted at 0° and 50% at 180°. The range of corrections calculated was 10–15% for one-proton emission, 5–18% for two-nucleon emission, and 3–18% for three-nucleon emission. These values represent upper limits of corrections, since the 0–180° angular distribution was assumed. For comparing the wide variety of reaction products of Fig. 1 with the theoretical range curve, the experimental ranges were decreased by the appropriate correction and compared with the range prediction of LSS. In comparing the experimental recoil ranges of specific reaction products with a theoretical range curve (in Figs. 2–5), the range-energy curve of LSS was modified, as discussed above, to represent the range expectation for full-momentum transfer reactions with subsequent particle evaporation symmetric about 90° c.m. (actually a 0–180° angular distribution).

C. Sensitivity of Range Measurements to Reaction Mechanism

The initial question in the application of recoil ranges to deducing reaction mechanisms (i.e., direct reactions versus compound nucleus) is the sensitivity of the mean

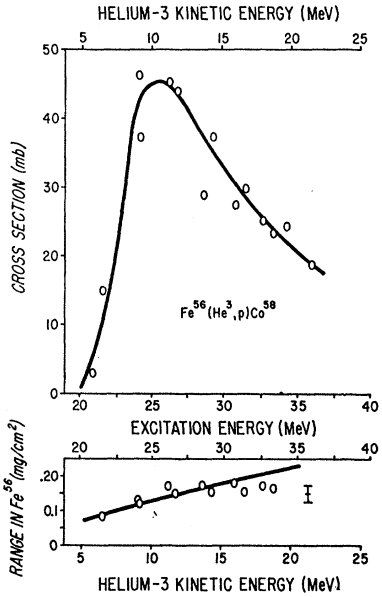

FIG. 2. Excitation function and recoil ranges resulting from the Fe^{56}(He^3,p)Co^{58} reaction. The experimental cross sections are plotted in the upper part of the figure, the corresponding recoil ranges are plotted in the lower section. A smooth curve has been drawn through the experimental cross sections to define the excitation function. The solid recoil-range curve is the theoretical-range expectation for products resulting from a compound-nucleus mechanism, as calculated with the theory of Lindhard *et al.* and corrected for the influence of nucleon evaporation as described in Sec. III. The error flag is an estimate of the uncertainty in the experimental recoil ranges, and does not represent an experimental measurement.

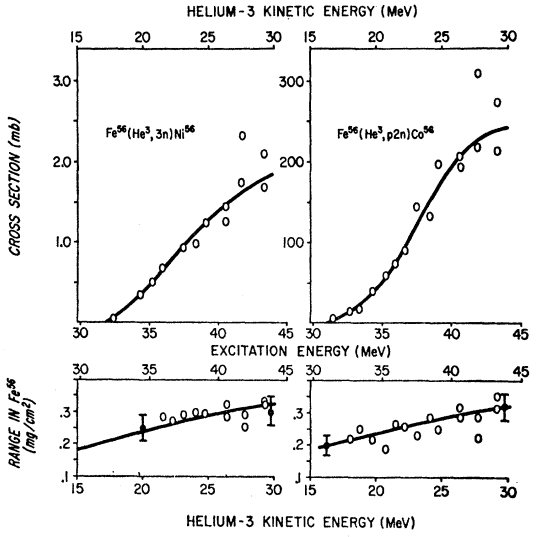

FIG. 3. Excitation functions and recoil ranges for the Fe^{56}-$(He^3,3n)Ni^{56}$ and $Fe^{56}(He^3,p2n)Co^{56}$ reactions. The significance of the points and curves is as given in Fig. 2. The error flags are estimates of experimental errors, and do not represent experimental measurements.

range to direct reactions. In reactions of the type $(\alpha,\alpha' xnyp)$, it was shown that the range was very sensitive to the symmetry about 90° of the emitted α particle.[7] This is unfortunately not the case for reactions in which only nucleons are emitted; here the decrease in range for direct reactions is more critically a function of the degree of asymmetry of the emitted particles.

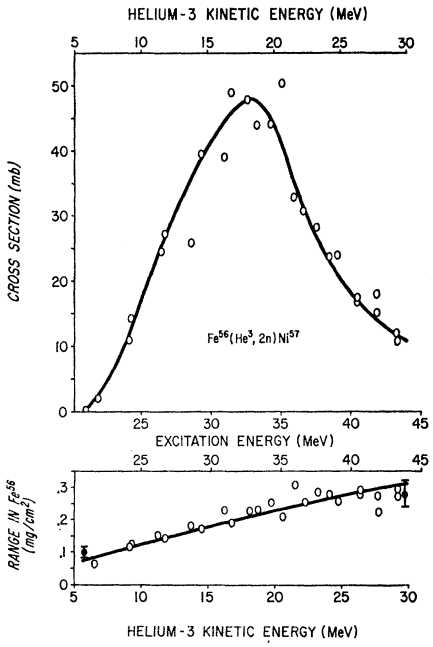

FIG. 4. Excitation function and recoil ranges for the Fe^{56}-$(He^3,2n)Ni^{57}$ reaction. The significance of the points and curves is as given in Fig. 2. The error flags are estimates of the experimental errors, and do not represent experimental measurements.

In the following paragraphs we attempt to give a semiquantitative estimate of the amount and types of direct interactions which are readily detectable from a range measurement.

In general, the published work on He^3 stripping reactions indicates a strong forward peaking for the particles which are not captured.[17–19] In these situations the recoil ranges would be sensitive to a significant admixture of stripping reactions with compound-nucleus reactions. In the following paragraph we quote the results of several arbitrary (but reasonable with respect to published results) calculations to justify the previous statement.

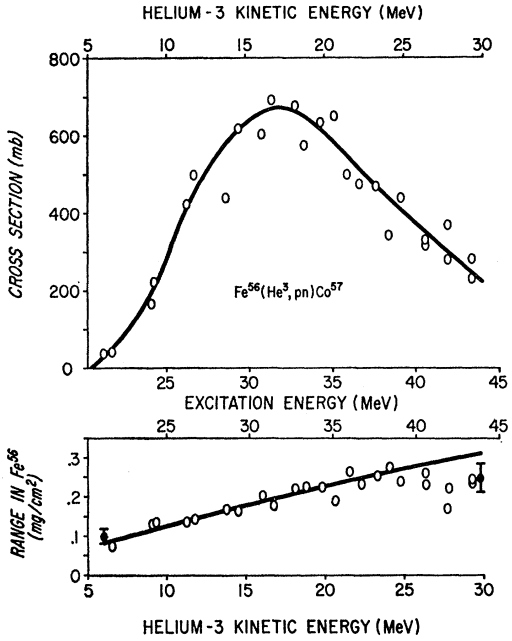

FIG. 5. Excitation function and recoil ranges for the Fe^{56}-$(He^3,pn)Co^{57}$ reaction. The significance of the points and curves is as given in Fig. 2. The error flags are estimates of the experimental errors, and do not represent experimental measurements.

Consider the $Fe^{56}(He^3,d)$ reaction at 15-MeV incident He^3 energy. Assuming a deuteron kinetic energy of 10 MeV and an emission angle of 45°, the calculated recoil range would be 30% of the average value calculated for full-momentum transfer. Thus, if 80% of the reactions proceeded by a compound nucleus mechanism, and 20% by the simplified direct interaction mechansim described above, the average range would be ≈85% of that expected for a pure compound-nucleus mechanism. We feel that a 15% discrepancy is the borderline of a significant deviation from the theoretical range curve, in view of the uncertainties in the theoretical range curve and experimental measurements. A similar

[17] D. A. Bromley and E. Almqvist, in *Reports on Progress in Physics*, edited by A. E. Stickland (The Physical Society, London, 1960), Vol. 23, p. 544.
[18] A. G. Blair and H. E. Wegner, Phys. Rev. **127**, 1233 (1962).
[19] H. E. Wegner and W. S. Hall, Phys. Rev. **119**, 1654 (1960).

calculation for proton or neutron emission, with $E_{He^3}=15$ MeV and $E_p=E_n=15$ MeV, indicates that if more than 25% of the reactions proceed by such a mechanism, the decrease in recoil range will be observable. Calculations in which the incident He^3 energy is varied, varying the particle emission energy by the same amount and keeping the average angle at 45°, give very similar values for the sensitivity of recoil ranges to reaction mechanism. We conclude from these calculations that recoil range measurements should reveal situations where more than $\approx 25\%$ of the reactions leading to a given product proceed by a mechanism characterized by a strong forward peaking of emitted particles.

D. Recoil Range Results

1. Discussion

Excitation functions and recoil ranges for the $Fe^{56}(He^3,p)Co^{58}$, $Fe^{56}(He^3,pn)Co^{57}$, $Fe^{56}(He^3,p2n)Co^{56}$, $Fe^{56}(He^3,2n)Ni^{57}$, and $Fe^{56}(He^3,3n)Ni^{56}$ reactions are shown in Figs. 2–5. All recoil ranges are apparently within experimental error of the calculated range curves corrected for nucleon emission, with the exception of the Co^{57} recoil products formed with He^3-ion kinetic energies greater than 25 MeV (Fig. 5). In this region, the excitation function has a large high-energy tail, and the recoil range shows a 25% decrease from the theoretical value. This would imply that the high-energy tail of the excitation function results largely from partial-momentum-transfer reactions and, therefore, should not be expected to be in agreement with the statistical theory predictions.

2. Conclusions

The $Fe^{56}(He^3,p)$ proton spectra and angular distributions showed that a preponderance of reactions were consistent with a compound nucleus mechanism for 10-MeV incident He^3 energy.[2] Extension of the Fe^{56} bombardments to higher He^3 energies yields reactions which are, according to the recoil range criterion, still consistent preponderately with a compound-nucleus mechanism [with an apparent exception being the high-energy tail of the $Fe^{56}(He^3,pn)Co^{57}$ reaction]. In view of these results, it would be worthwhile and meaningful to compare the experimental excitation functions of this work with the predictions of the statistical theory.

IV. STATISTICAL THEORY

A. Evaluation of the Weisskopf Evaporation Formula

The calculations performed in this work are based on the statistical theory as formulated by Weisskopf[3] for a system having no angular momentum restrictions on the decay of compound nuclei,

$$P_\nu(\epsilon)d\epsilon \propto \gamma_\nu \epsilon \sigma_\nu(\epsilon)\frac{\rho(E_f)}{\rho(E_i)}d\epsilon, \tag{5}$$

where $P_\nu(\epsilon)d\epsilon$ is the probability of emitting a particle ν with channel energy between ϵ and $\epsilon+d\epsilon$, $\gamma_\nu=(2S+1)\mu$ (where S is the spin and μ the reduced mass of the particle ν), $\sigma_\nu(\epsilon)$ is the inverse reaction cross section for the particle ν with channel energy ϵ, and $\rho(E_f)/\rho(E_i)$ represents the ratio of level densities of the final to the initial state. Equation (5) gives the relative probability of decay for a nucleus at a given excitation energy; the value of the integral over all emission energies and the sum over all emitted particles is a function of the initial excitation energy. In any calculation involving multiple-particle emission, one is dealing (after the first emission) with a spectrum of energies, and normalization of Eq. (5) is necessary. To emphasize this, and since the level density of the compound nucleus, $\rho(E_i)$, cancels in any calculation, we may rewrite Eq. (5) in the normalized form used for computer evaluation,[5]

$$P_\nu(\epsilon)d\epsilon=\frac{\gamma_\nu \epsilon \sigma_\nu(\epsilon)\rho(E_f)d\epsilon}{\left(\sum_{\nu=1}^{n}\gamma_\nu\int_{\epsilon=0}^{\infty}\epsilon\rho(E_f)\sigma_\nu(\epsilon)d\epsilon\right)}. \tag{6}$$

The computer programs used to evaluate Eq. (6) have been described previously.[20,21] In these calculations competition due to n,p, and α emission was considered; it has been shown that competition due to d, t, and He^3 evaporation is not significant at the excitation energies encountered in this work.[22]

We have assumed a Fermi gas level density[23,24] in evaluating Eq. (6),

$$\rho(E)\propto E^{-2}e^{2(aE)^{1/2}}. \tag{7}$$

The excitation energies were adjusted for odd-even effects, as will be discussed. Equations (6) and (7) were used in one set of calculations to be presented in the next section.

Implicit in the use of Eqs. (6) and (7) is the assumption that

$$\rho(E,J)\propto(2J+1)\rho(E), \tag{8}$$

i.e., there is no restriction on available spin states in residual nuclei.[25] A more realistic level-density relationship is

$$\rho(E,J)\propto(2J+1)\rho(E)\exp(-J^2/2\sigma^2), \tag{9}$$

where σ^2 is the (temperature-dependent) spin-cutoff parameter.[26] A rigorous calculation using Eq. (9) with proper treatment of angular-momentum coupling and available angular-momentum phase space would be

[20] M. Blann and G. Merkel, Phys. Rev. **131**, 764 (1963).
[21] M. Blann and G. Merkel, Nucl. Phys. **52**, 673 (1964).
[22] M. Blann, Phys. Rev. **133**, B707 (1964).
[23] T. Ericson, in *Proceedings of the International Conference on Nuclear Structure, Kingston, Canada, 1960*, edited by D. A. Bromley and E. Vogt (University of Toronto Press, Toronto, 1960), p. 697.
[24] D. W. Lang, Nucl. Phys. **26**, 434 (1961).
[25] T. Ericson, in *Advances in Physics*, edited by N. F. Mott (Taylor and Francis, Ltd., London, 1960), Vol. 9, p. 425.
[26] T. Ericson and V. Strutinski, Nucl. Phys. **8**, 284 (1958).

impractical with the computers presently available. We have, therefore, performed a second set of calculations in which a simplified model was used to gain insight into the results of a more rigorous calculation. We describe this model in Sec. IV B.

B. Angular-Momentum-Dependent Model of Nuclear Decay

Physically, the model used for the second set of calculations may be thought of as a system in which the compound nuclei undergo classical rotation for each contributing impact parameter; the angular momentum is assumed to be tied up as rotational energy of a rigid rotor, and it is assumed that the rotational energy remains unchanged throughout the evaporation cascade. The calculation is, therefore, one in which Eq. (6) is evaluated with a spectrum of compound-nucleus energies, rather than a discrete value, i.e.,

$$E_{\text{compound nucleus}}=\sum_{J=0}^{\infty}[(2J+1)T_J]\times(E_i-J(J+1)\hbar^2/2I_{\text{RIG}}), \quad (10)$$

where E_i represents the compound-nucleus excitation energy with zero rotational energy, T_J is the transmission coefficient for formation of the compound nucleus with angular momentum J, and I_{RIG} is the rigid-body moment of inertia. We assumed $R_0=1.2\text{F}$ in calculating I_{RIG}.

As described above, we have calculated cross sections in the second set of calculations with the equations

$$P_\nu(J,\epsilon)d\epsilon=\frac{\gamma_\nu\sigma_{\nu\epsilon}(\epsilon)\rho(E-J(J+1)\hbar^2/2I_{\text{RIG}})d\epsilon}{\sum_\nu\gamma_\nu\int_0^\infty\sigma_{\nu\epsilon}(\epsilon)\rho(E-J(J+1)\hbar^2/2I_{\text{RIG}})d\epsilon} \quad (11)$$

and

$$\sigma_{\text{PRODUCT}}(\epsilon)d\epsilon=\pi\lambda\!\!\!^{-2}\sum_{J=0}^{\infty}(2J+1)T_JP_\nu(J,\epsilon)d\epsilon. \quad (12)$$

The level density of Eq. (11) may be related to Eq. (9): Remembering that $\sigma^2=(IT/\hbar^2)$, Eq. (9) may be rewritten as

$$\rho(E,J)\propto(2J+1)\rho(E)\exp\left(\frac{-J^2\hbar^2}{2IT}\right) \quad (13)$$

or the corresponding quantum-mechanical form may be written with $J(J+1)$ replacing J^2. Recalling the definition of nuclear temperature and provided E_{ROT} is small compared with E we can write

$$\rho(E)\exp(-E_{\text{ROT}}/T)\simeq\rho(E-E_{\text{ROT}}). \quad (14)$$

The model described above neglects the strong coupling[25,26] between **J** of the residual nucleus and **l** of the emitted particle which may be expected if $(Jl/\sigma^2)\geq 1$. The model should be valid in the limit of weak coupling. The relationship of the model to the theoretical description of Ericson and Strutinski has been discussed previously.[27]

C. Influence of Shell Occupation on Level Densities

Many excitation functions have been measured in the region of the 28-nucleon closed shell.[6,16,21,28,29] A common feature of these reactions is an anomalously low yield for the doubly closed shell Ni^{56} and closed-shell Ni^{57} nuclides. It has been suggested that the low yields may be attributable to the influence of the 28-nucleon shell on level densities.[21,29] Margenau suggested that such an effect may be present as a statistical consequence of shell-occupation number.[30] The argument is that in a closed shell there is only one combination of particles in the ground state, while in a partially filled degenerate shell of X particles and Y holes there are $(X+Y)!/X!Y!$ combinations of particles and holes. Margenau showed further that this effect should persist to excitations considerably above the ground state.

Rosenzweig has derived a closed-form level-density expression in which the shell effect described above may be reproduced by a shift in ground-state energy; the model used in the derivation was a Fermi-gas model in which the spacing γ of all neutron levels is equal, as is the degeneracy g. The degeneracy e and spacing ϵ of all proton levels is also assumed to be equal.[31] The energy shift is given by

$$\Delta E=\frac{g\gamma}{12}-\frac{\gamma}{2g}(n-g/2)^2+\frac{e\epsilon}{12}-\frac{\epsilon}{2e}(p-e/2)^2, \quad (15)$$

where n and p represent, respectively, the number of neutrons and protons in the Fermi level. We have performed a third set of calculations with Eqs. (6) and (7) with excitation energies shifted according to Eq. (15) to estimate the influence of shell structure on level densities.

D. Parameter Evaluation

In the calculations described, using Eqs. (6), (7), (12), and (15), we have tried to use independently determined parameters rather than vary parameters to get the best fit. We discuss the selection of parameters in the following paragraphs.

1. Level-Spacing Parameter a

The level-spacing parameter used was $a=8.7\ \text{MeV}^{-1}$, a value determined from proton spectra resulting from the bombardment of Fe^{56} with 10-MeV He^3 ions.[2] This

[27] M. Blann and G. Merkel, Phys. Rev. **137**, B367 (1965).
[28] F. S. Houck and J. Miller, Phys. Rev. **123**, 231 (1961).
[29] R. A. Sharp, R. M. Diamond, and G. Wilkinson, Phys. Rev. **101**, 1493 (1956).
[30] H. Margenau, Phys. Rev. **59**, 627 (1941).
[31] N. Rosenzweig, Phys. Rev. **108**, 817 (1957).

TABLE III. Summary of optical-model parameters used in calculating nonelastic cross sections.

Incident particle	Radius parameter (F)	Projectile size (F)	Diffuseness parameter (F)	Real potential depth (MeV)	Imaginary potential depth (MeV)	Reference to source of parameters and general details not listed in this table
n	1.25	0	a	52	20	a
p	1.25	0	not constant[a]			a
α	1.14	2.24	0.50	49.3	11	a
He^3	1.52	0	0.61	68	14	b

[a] Reference 36; a real spin-orbit depth of 33 MeV was used in these calculations. For charged particles, a square-well charge distribution was used.
[b] Reference 37; a square-well charge distribution was used.

value is considerably higher than the value $a=7.0$ MeV^{-1} determined by Sherr and Brady[32] from $Ni^{58}(p,\alpha)$ spectra (19-MeV protons) and by Benveniste *et al.* in the $Fe^{56}(\alpha,\alpha')$ reactions (21, 27, and 44 MeV-helium ions).[33] In all three sets of experiments the spectral data were analyzed with a level-density expression as given by Eq. (7). Since there is a discrepancy in the two values of a, we have repeated all calculations with $a=7.0$ MeV^{-1}. Results of the first set of calculations will be presented in the next section; where any significant change results from using $a=7.0$ MeV^{-1}, the difference will be stated.

2. Pairing energy δ

The odd-even influence on level densities has been corrected for by a shift in ground-state energies, as suggested by Hurwitz and Bethe.[34] We have taken the "energy gap" to be equal to the pairing energy δ. The pairing energy was evaluated as the difference between even-A mass parabolas in the $A=60$ region, using the masses of Everling *et al.*[35] The energy shifts found were 1.4 MeV for odd-A nuclei and 2.8 MeV for even-even nuclei.

3. Inverse-Reaction Cross Sections

Inverse-reaction cross sections were calculated using the nuclear optical model. It was assumed that

$$\sigma(\epsilon,E^*)=\sigma_{\text{nonelastic}}(\epsilon,0)\,, \tag{16}$$

where $\sigma(\epsilon,E^*)$ represents the cross section for capture of a particle of kinetic energy ϵ into a nucleus at excitation energy E^*, and $\sigma_{\text{nonelastic}}(\epsilon,0)$ represents the nonelastic cross section for capture of the same particle of kinetic energy ϵ into a nucleus in its ground state. The computer code of Bjorklund and Fernbach was used in these calculations. The optical-model parameters used were taken from the literature,[36] with the exception of values for neutron inverse cross sections; the latter values were chosen from the literature but with an imaginary potential which was arbitrarily deepened to approximate an increased opacity for highly excited nuclei.[25,36] The numerical values of the parameters used are summarized in Table II. The approximations involved in using optical-model nonelastic cross sections for inverse-reaction cross sections have been discussed in a prior publication.[20]

4. Compound-Nucleus-Formation Cross Section

The capture cross section for formation of the compound nucleus was assumed to be the total nonelastic cross section as calculated with the nuclear optical model. The parameters used[37] are listed in Table III. For the calculations described by Eqs. (7) and (8), the transmission coefficients from the optical-model calculations were used.

5. Parameter Values for Shell-Occupation Correction.

The values necessary for calculating energy shifts with Eq. (15) are the spacings between neutron levels and between proton levels, and the degeneracies of the levels. The nuclei investigated in this work are filling the $f_{7/2}$ and $p_{3/2}$ levels; consequently we have used an average degeneracy of 6 for both neutron and proton levels. The spacing between the levels was taken from the Nilsson level schemes,[38] and was 3 MeV. With these values, Eq. (15) simplifies to

$$\Delta E=3-[(n-3)^2/4]-[(p-3)^2/4].$$

V. RESULTS AND DISCUSSION

The experimental excitation functions for the (He^3,p), (He^3,pn), $(He^3,p2n)$, $(He^3,2n)$, and $(He^3,3n)$ reactions of Fe^{56} are presented in Fig. 6. The results of the statistical-theory calculations described in Sec. IVA are also shown in Fig. 6. Several generalizations may be made: The magnitudes of calculated excitation functions are incorrect; the calculated curves attain their maxima at too low an excitation energy, and, for reactions producing Ni^{57}, Co^{57}, and Co^{58}, the calculated

[32] R. Sherr and F. P. Brady, Phys. Rev. **124**, 1928 (1961).
[33] J. Benveniste, G. Merkel, and A. Mitchell, Bull. Am. Phys. Soc. **7**, 454 (1962).
[34] H. Hurwitz and H. Bethe, Phys. Rev. **81**, 898 (1951).
[35] F. Everling, L. A. König, J. H. E. Mattauch, and A. H. Wapstra, Nucl. Phys. **18**, 529 (1960).
[36] F. E. Bjorklund and S. Fernbach, in *Proceedings of the Second United Nations International Conference on the Peaceful Uses of Atomic Energy, Geneva, 1958* (United Nations, Geneva, 1958), Vol. 14, p. 24.
[37] G. R. Satchler (private communication).
[38] S. C. Nilsson, Kgl. Danske Videnskab. Selskab, Mat. Fys. Medd. **29**, No. 16 (1955).

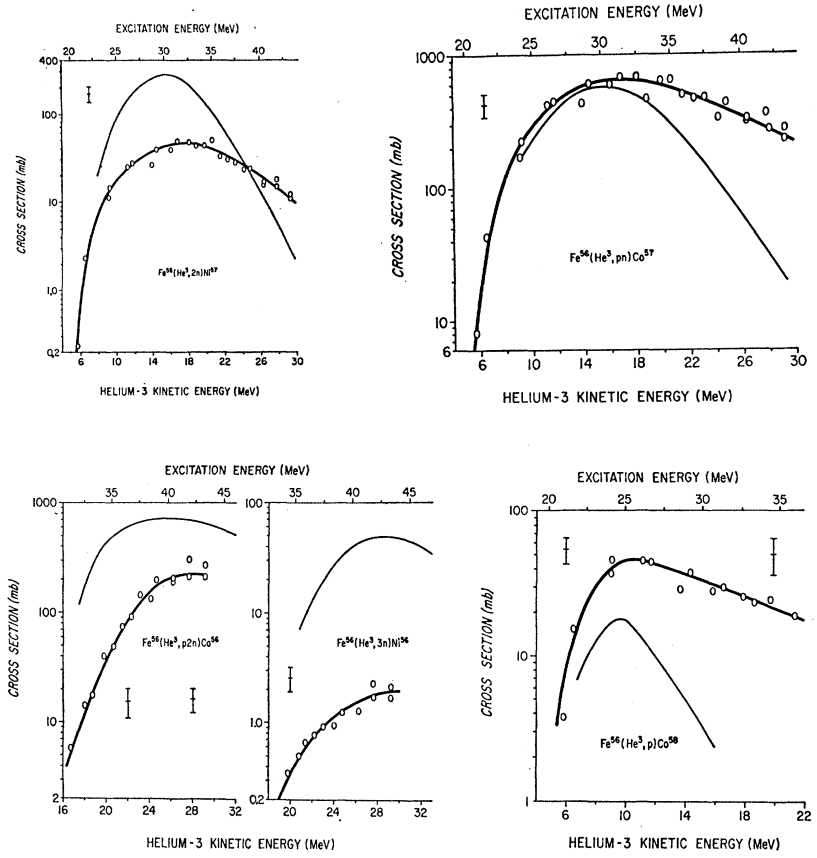

FIG. 6. The experimental excitation functions for the reactions listed are compared with the standard statistical-theory calculations. The open points represent the experimental yields. A smooth solid curve has been drawn through the experimental yields to aid in visual definition of the excitation functions. The error flags give the estimated uncertainties in the experimental yields; because of the method of analysis, the uncertainties in the yields of Co^{56} and Co^{58} are a function of energy, as indicated. The solid curves (not drawn through the experimental points) represent results of the calculations of Sec. IV A.

yields decrease too rapidly with increasing energy past the excitation function maxima. Recoil-range measurements show evidence that the yields of Co^{57} resulting from bombardment with He^3 ions in excess of 22-MeV kinetic energy may have significant contributions from direct-interaction processes. Recoil ranges for Co^{58} are inconclusive, while the ranges for Ni^{57} are consistent with a compound-nucleus mechanism over the entire energy range. We might, therefore, expect better agreement at higher energies in the shapes of calculated and experimental excitation functions for the production of Ni^{57}. In the remainder of this section we will discuss the relationship of the failures of the calculations shown in Fig. 6 to the physical effects discussed in Secs. IVB and IVC.

It has been suggested that a result of angular-momentum conservation may be an enhancement of γ-ray emission in competition with particle emission.[39] Qualitatively, as an excited nucleus decays by particle emission, a point may be reached in the evaporation cascade where, because of an exponentially decreasing probability of finding a state of high J, the next nucleon to be emitted has sufficient energy available for emission but can find no allowable spin state in the residual nucleus. In such a situation radiative de-excitation would take place. Stated in other terms, there is for each spin J a lowest lying level at energy E_J. The relationship between J and E_J is an open question; Grover[40] and Sperber[41] have suggested (from statistical considerations) that

$$E_J \propto \frac{J(J+1)\hbar^2}{2I}, \tag{17}$$

where I is the nuclear moment of inertia. In any case,

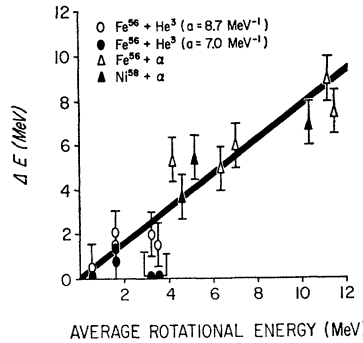

FIG. 7. The shifts in energy ΔE between calculated and experimental excitation-function maxima vs the average rotational energy of the compound nuclei for α-induced reactions of Ni^{58} and Fe^{56}, and He^3-induced reactions of Fe^{56}. The error bars are estimates of the uncertainties in the positions of the experimental excitation-function maxima.

[39] J. R. Grover, Phys. Rev. **123**, 267 (1961).

[40] J. R. Grover, Phys. Rev. **127**, 2142 (1962).

[41] D. Sperber, thesis, Princeton University, 1961 (unpublished).

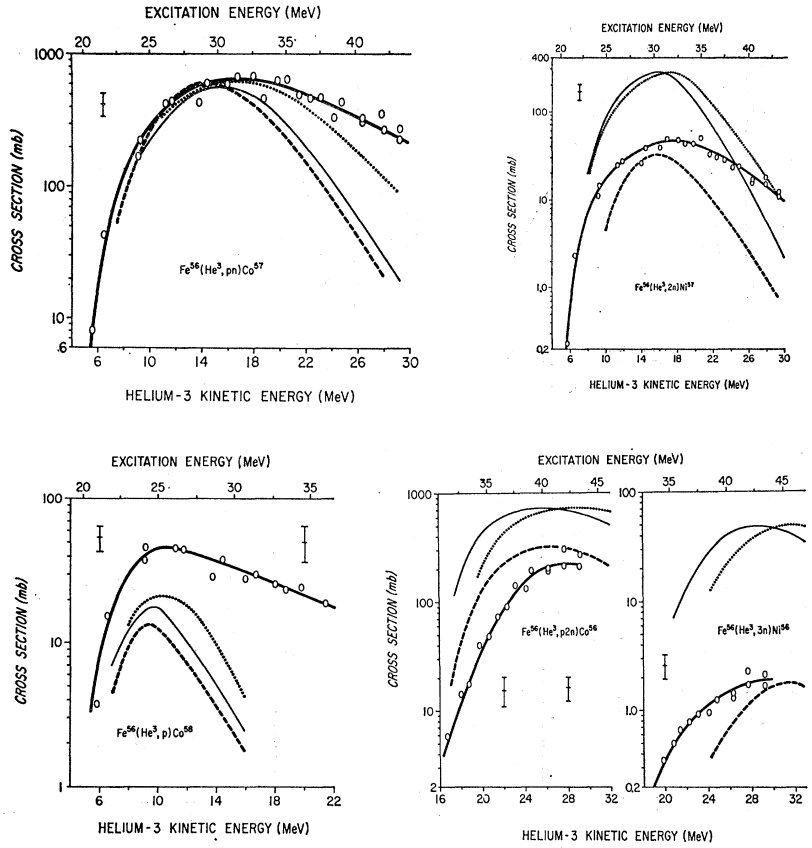

FIG. 8. The solid curves and open points have the same significance as in Fig. 6. The dotted curves represent excitation functions calculated with the rotational model described in Sec. IV B. The dashed curves represent excitation functions calculated with Rosenzweig's model to estimate the influence of shell occupation on level densities, as described in Sec. IV C.

if E_J is a monotonic function of J, γ-ray emission should be a function of rotational energy. The shift in energy between calculated and experimental excitation functions would, therefore, show a correlation with the rotational energy of the experimental system. We have looked for such a correlation as follows: For the reactions of this work and for the α-induced reactions of Fe^{56} and Ni^{58}, we have measured the displacement in energy, ΔE, between the maxima of calculated and experimental excitation functions.[16] These values have been plotted in Fig. 7 against the average rotational energy, $\bar{E}_{\mathrm{ROT}}$, of the compound nuclei as calculated with optical-model transmission coefficients and defined by

$$\bar{E}_{\mathrm{ROT}}=\sum_{J=0}^{\infty}(2J+1)T_J(J+1)J\hbar^2/2I_{\mathrm{RIG}} \times\left[\sum_{J=0}^{\infty}(2J+1)T_J\right]^{-1}. \quad (18)$$

The error bars on the points of Fig. 7 are estimates of the uncertainties in the positions of the experimental excitation-function maxima. The solid line has been drawn in solely as a visual aid in emphasizing that there is a correlation between ΔE and $\bar{E}_{\mathrm{ROT}}$. We have overlooked factors such as increased particle kinetic energy due to high angular momentum (which classically might decrease ΔE by 10–20%), and the overestimation of $\bar{E}_{\mathrm{ROT}}$ due to using optical model T_J (which include contributions from inelastic scattering). The purpose of Fig. 7 is only to show that, to first order, the discrepancy between positions of calculated and experimental excitation functions is consistent with the explanation offered above. Values of ΔE for He^3-induced reactions of Fe^{56} calculated with $a=7.0$ MeV^{-1} are also shown in Fig. 7; the conclusions are unchanged.

Results of a second set of calculations, in which the influence of angular momentum on level densities and γ-ray de-excitation was considered as described in Sec. IV B, are presented in Fig. 8. The calculated excitation functions are shifted to a higher excitation energy, and broadened with respect to the calculations of Sec. IVA. The positions (on the energy axis) of the maxima of the second set of calculations are in better agreement with the experimental values than those of the first set of calculations, consistent with the observation in reactions of Ni^{58} and Fe^{56} with 20–68-MeV $^4He^{2+}$ ions.[27,42] The second set of calculations also predicts a greater compound-nucleus contribution to the "high-energy tail" of the excitation functions, although there is not a sufficient increase to give agreement with the experimental observations.

In the third set of calculations (Sec. IVC) we have attempted to consider the influence of shell-occupation

[42] A. Ewart, thesis, University of Rochester, 1964 (unpublished).

TABLE IV. Measured and calculated yield ratios for the production of Co^{56}, Ni^{56}, Co^{57}, and Ni^{57}.

Reactions	Experimental ratio[a]	Calculated ratio[a]	(Experimental ratio)/(Calculated ratio)	Calculated ratio with shell correction[a]	(Experimental ratio)/(Calculated ratio with shell correction)
$\frac{Fe^{56}(He^3,pn)Co^{57}}{Fe^{56}(He^3,2n)Ni^{57}}$	14.5	2.1	7.0	16.7	0.82
$\frac{Fe^{56}(He^3,p2n)Co^{56}}{Fe^{56}(He^3,3n)Ni^{56}}$	125	15	8.3	170	0.74

[a] Measured at excitation function maxima.

effects on level densities, as suggested by Rosenzweig. This was done in an attempt to find an explanation for the low experimental yields of Ni^{56} and Ni^{57} observed in this work, and in other work in which these isotopes are produced. The results of these calculations are presented in Fig. 8; the results are summarized in Table IV for the isobaric pairs Co^{56}, Ni^{56}, and Co^{57}, Ni^{57}. We exclude the Co^{58} excitation function from further discussion since the origin of the discrepancy between calculated and experimental values is uncertain; the magnitude of the calculated excitation function is very sensitive to its position on the energy axis, since the compound-nucleus-formation cross section is decreasing very rapidly in the region of the Co^{58} excitation function peak. This ambiguity is not present for the other excitation functions, since the excitation energies required for two- or three-particle emission are sufficiently high that the compound-nucleus-formation cross section varies only slowly with energy.

The values cited in Table IV are given as ratios of isobaric yields, so that uncertainties in the magnitude of the compound-nucleus cross section would cancel. This was done because the interest in these calculations is in the relative level densities of the nuclides in question. Table IV shows that inclusion of the Margenau-Rosenzweig effect in the calculation of level densities greatly improves the agreement between calculated and experimental excitation functions, in this case from a disagreement of a factor of 7–8 to agreement within experimental uncertainties. Similar improvements have been noted for calculation of the $Ni^{58}(\alpha,\alpha n)Ni^{57}$, $Ni^{58}(\alpha,\alpha p)Co^{57}$, $Ni^{58}(\alpha,\alpha 2n)Ni^{56}$, $Ni^{58}(\alpha,\alpha pn)Co^{56}$, $Fe^{56}(\alpha,3n)Ni^{57}$, $Fe^{56}(\alpha,p2n)Co^{57}$, $Fe^{56}(\alpha,4n)Ni^{56}$, and $Fe^{56}(\alpha,p3n)Co^{56}$ excitation functions.[27,42] The consistent and drastic improvement in all these calculations resulting from the use of Rosenzweig's model is evidence for the existence of the Margenau-Rosenzweig effect in the $f_{7/2}$ shell.

VI. CONCLUSIONS

With the exceptions noted in Sec. III D, the recoil ranges of this work show the excitation functions to be consistent with a compound-nucleus mechanism. Comparison of the results with statistical-theory calculations is therefore justified.

The standard statistical-theory calculation described in Sec. IVA does not satisfactorily reproduce the peak position, shape, or magnitude of the experimental excitation functions of this work. Figure 7 indicates that a correlation exists between the discrepancies in the energy of the calculated and experimental excitation-function maxima and the average rotational energy of the systems [$(Fe^{56}+He^3)$, $(Fe^{56}+\alpha)$, and $(Ni^{58}+\alpha)$]. The correlation noted is consistent with the argument of increased γ-ray competition with particle emission for systems of high-angular momentum. More extensive correlations of the type given in Fig. 7 may yield empirical evidence on the relationship between E_J and J.

The second set of calculations, in which the influence of angular momentum on level densities and γ-ray emission was considered as described in Sec. IVB, yielded somewhat improved agreement with experimental values with respect to the position (on the energy axis) of the excitation-function maxima, and shape.

In the third set of calculations the influence of shell-occupation number on level densities was considered, using the model suggested by Rosenzweig.[31] This set of calculated excitation functions gave yields which were in better agreement with experimental results by an order of magnitude, as is summarized in Table IV. This is evidence for the presence of the Margenau-Rosenzweig effect in the region of the $f_{7/2}$ shell, consistent with similar evidence for other systems ($Fe^{56}+\alpha$ and $Ni^{58}+\alpha$).

ACKNOWLEDGMENTS

It is our pleasure to acknowledge the assistance and cooperation of Dr. I. Preiss, Professor M. Baranger, and the crew of the Yale Heavy Ion Linear Accelerator in obtaining the bombardments described in this work. We are grateful to T. Pierce and R. Sorbo for help with the chemical separations.

The authors are pleased to acknowledge the cooperation and hospitality of Dr. M. Goldstein and Dr. H. Mullish of the New York University Computing Center (Atomic Energy Commission Computing Center) in performing the calculations of this work. The financial support of the AEC, and the College of Arts and Science of the University of Rochester is also gratefully acknowledged.